

THE IMPACT OF THE HYDROGEN SPECIES ON THE HHFW PERFORMANCE WITH POSSIBLE NEW NSTX-U SCENARIOS

N. BERTELLI¹, M. ONO¹, J. E. JAEGER², R. HARVEY³, Y. PETROV³, E. J. VALEO¹, R. J. PERKINS¹, J. C. HOSEA¹, and E.-H. KIM¹

¹Princeton Plasma Physics Laboratory, Princeton, NJ, USA

²XCEL Engineering Inc., Oak Ridge, TN, USA

³CompX, Del Mar, CA, USA

Corresponding author e-mail: nbertell@pppl.gov

Abstract

The main goal of the NSTX-Upgrade (NSTX-U) is to operate at toroidal magnetic field at magnetic axis $B_T=1T$. With this magnetic field, the first and second harmonics of hydrogen (H) are located at the high-field side and in the core plasma, respectively. As a consequence, part of the high-harmonic fast-wave (HHFW) injected power can be absorbed by the H population. This condition could open up new HHFW scenarios, which in turn can be relevant for the initial ITER ICRH experiments. Therefore, in this work, we analyze in detail all these possible scenarios by the use of the full wave code AORSA. AORSA simulations have been performed for NSTX-U $B_T=1T$ plasma with different H concentrations (from 1% to 10%) with and without NBI. For $f=30\text{MHz}$ and $B_T=1T$, unlike an on-axis power deposition for electrons and fast ions, a localized H absorption around the second cyclotron H harmonic is observed by AORSA. For larger wave toroidal number, n_ϕ , the electron damping is dominant. However, for $n_\phi=5$ and 10% H concentration, up to 30% and 60% of the total power can be absorbed by H population with and without NBI, respectively. The impact of H species is less significant for $f=60\text{MHz}$, however, fast ions absorption can be strong particularly for lower n_ϕ . A magnetic field scan is also presented showing a gradually increase of H absorption with higher magnetic field.

1. INTRODUCTION

The NSTX-Upgrade (NSTX-U) project [1-4] consists of two main elements: (i) a new and more powerful center-stack and (ii) a tangentially-aimed second NBI system. NSTX-U aims to double the magnetic toroidal field at the magnetic axis from $B_T\sim 0.5\text{ T}$ to 1 T, the plasma current from $I_p\sim 1\text{ MA}$ to 2 MA, and the NBI heating and current drive power up to 10 MW. Beyond these new capabilities NSTX-U retains the previous 6 MW High-Harmonic Fast Wave (HHFW) system for heating and current drive [5, 6]. The use of HHFW in NSTX-U will be focused on (i) the ramp-up phase in order to increase the electron temperature and the plasma current sufficient for the NBI injection and (ii) the flat-top plasma sustainment phase with or without neutral beam injection (NBI). HHFW experiments in NSTX showed very high electron temperatures for L-mode plasmas when an internal transport barrier was formed [7, 8]. On the other hand, it was found more challenging to heat H-mode plasma in combination with NBI. However, some cases of incremental HHFW heating of H-mode with NBI have been observed [9]. In this work, we are mainly focused on the flat-top phase for NSTX-U plasma with $B_T=1\text{ T}$. In particular, we investigate the impact of the hydrogen (H) species on HHFW performance in NSTX-U plasmas as the second harmonic layer of H is located in the core plasma (see next Section). The injected HHFW power absorbed by H species can affect the electron and/or the fast-ion heating with respect to the “standard” HHFW performance in NSTX. Moreover, the presence of the H species might have some positive effects: the presence of the second cyclotron harmonic of hydrogen in the core plasma can cause a localized H power absorption, which in turn could modify the ion temperature. This condition might open up new HHFW scenarios in NSTX-U, which in turn can also be relevant for the initial ITER experiments with 10 MW of ICRH during the hydrogen plasma phase. Here we analyse several scenarios by the use of the full wave code AORSA performing a scan in H concentration and the impact of different amplitude of magnetic field for two wave frequencies, $f=30$ and 60 MHz. Finally, a summary is provided in Section 3.

2. NUMERICAL RESULTS

2.1. The full wave code AORSA

AORSA is a full-wave code, which solves the Helmholtz wave equation for a tokamak geometry. In this work we are focused on the core plasma so we do not employ the AORSA extension, which including the scrape-off region beyond the last closed flux surface where the magnetic field lines are open [10-14]. However, in this

work we use the latest AORSA version where a new plasma dispersion function has been implemented including a more accurate physics for the electron Landau damping and a reduce numerical pollution for strong electron Landau damping cases [15]. AORSA includes the complete non-local, integral operator for the dielectric tensor that is valid for “all orders”, by taking into account all contributions in $k_{\perp}\rho_i$ ($k_{\perp}\rho_i$ are the perpendicular component of the wave vector relative to the local equilibrium magnetic field and the ion Larmor radius, respectively). This is essential for NSTX-U HHFw in which the ion Larmor radius is larger than the perpendicular wavelength and the ion-cyclotron harmonic number is large. AORSA utilizes a Fourier decomposition in the Cartesian coordinates x and y (in the poloidal plane) and in the toroidal direction of symmetry (ϕ), $\exp(in_{\phi}\phi)$ (n_{ϕ} is the toroidal mode number). More details of the AORSA code are found in Reference [10].

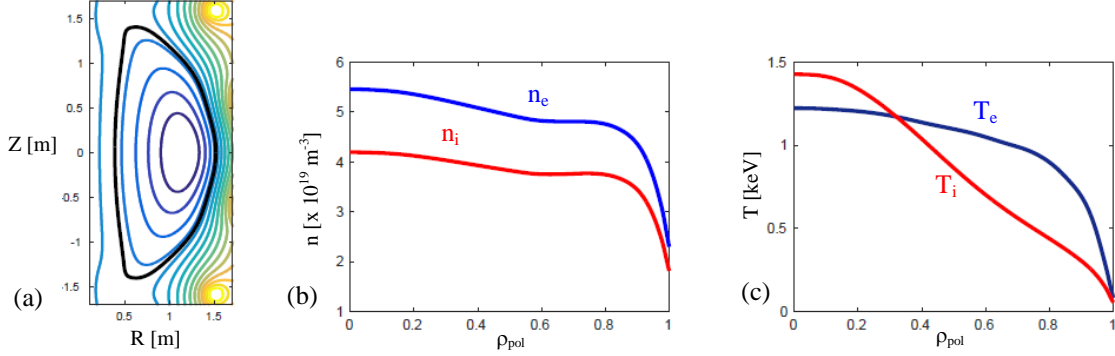


FIG. 1. Magnetic equilibrium (Fig. (a)), density (Fig. (b)), and temperature (Fig. (c)) profiles of electron (blue line) and the thermal deuterium (red line) as a function of the square root of the normalized poloidal flux, ρ_{pol} .

2.2. NSTX-U scenario(s) considered

The NSTX-U scenario considered is shown in Figure 1. Figure 1(a) shows the magnetic flux surfaces whereas Figures 1(b) and 1(c) show the plasma kinetic profiles. In particular, Figure 1(b) shows the electron (blue line) and ion (red line) density profiles as a function of the square root of the normalized poloidal flux, ρ_{pol} . Figure 1(c) shows the electron (blue line) and the ion (red line) temperature profiles as a function of ρ_{pol} . In this analysis we assume the same temperature profile for thermal ion species (deuterium, hydrogen, and carbon), while for the beam ions temperature (T_{beam}) we have adopted an effective temperature (namely, an equivalent Maxwellian) given by $T_{\text{beam}} = 2/3(E/n_{\text{beam}})$, where E and n_{beam} are the total energy density profile and the density of the beams ions, respectively. Both these quantities are provided by the TRANSP simulation [16, 17]. We consider two wave frequency regimes in the simulations: (i) $f=30$ MHz, which corresponds to the frequency of the current HHFw heating system, and (ii) $f=60$ MHz that have different D & H cyclotron resonances in the plasma. For $B_T=1$ T and $f=30$ MHz, the first and second harmonics of hydrogen (H) are located at the high-field side and in the core plasma, respectively (see Figure 2(a)). Moreover, for a $B=1$ T plasma, doubling the current wave frequency would reproduce a scenario already adopted in NSTX (at least, in terms of H & D cyclotron resonances in the plasma) as shown in Figures 2(b) and 3. From Figure 3, it is important to note the high number of deuterium cyclotron resonances present in the plasma generating a strong interaction between fast ions and HHFw, as observed experimentally [18, 19]. In order to investigate the impact of H species on the power partitioning among electron, thermal ions, and fast ions, four values (1, 2, 5, and 5%) of the H concentration are considered in the AORSA simulations with and without NBI and for $f=30$ and 60 MHz.

2.3. Hydrogen absorption for NSTX-U B = 1 T plasma

Figure 4 shows the wave electric field propagation for the NSTX-U plasma shown in figure 1. In particular, figures 4(a) and 4(b) show the real part of the right-handed wave electric field, $\text{Re}(E)$ and left-handed wave electric field, $\text{Re}(E_+)$ respectively, for $n_{\phi}=-12$ and assuming 10% H concentration. The black and white curves represent the last closed flux surface and the fast wave cut-off, respectively. Figure 5 shows the 2D contour plot of the electron (figure 5(a)), hydrogen (figure 5(b)), and fast ions (figure 5(c)) power deposition for NSTX-U plasma shown in figure 1 with $n_{\phi}=-12$ and $f=30$ MHz assuming a 10% H concentration. The electron power deposition is quite broad, from the outboard (just inside the last closed flux surface) and the core plasma, whereas the H power deposition is clearly localized around the second H cyclotron resonance, which is, in this

specific case, located just inboard with respect to the magnetic axis (see also figure 2(a)). It should be noted that the fundamental H power deposition is minimal because of the poor wave accessibility. In fact, from figure 4 you can see a weak electric field at the location of the first H cyclotron resonance. Unlike the power absorbed by electron, fast ions power deposition (D-NBI) is localized mainly around the fourth and fifth D cyclotron resonances.

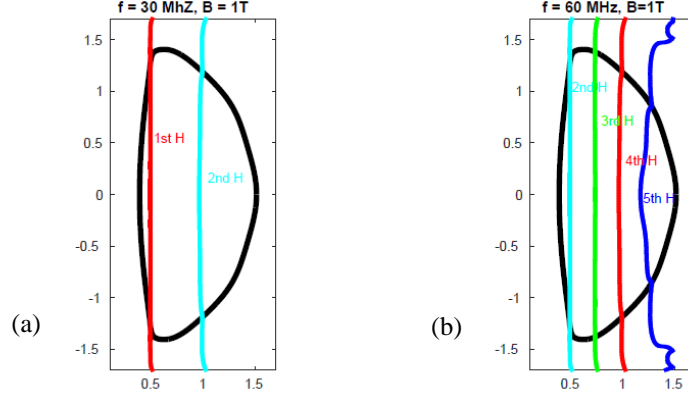


FIG. 2. Hydrogen (H) cyclotron resonances for an NSTX-U $B = 1$ T plasma assuming $f = 30$ MHz (Figure (a)) and 60 MHz (Figure (b)).

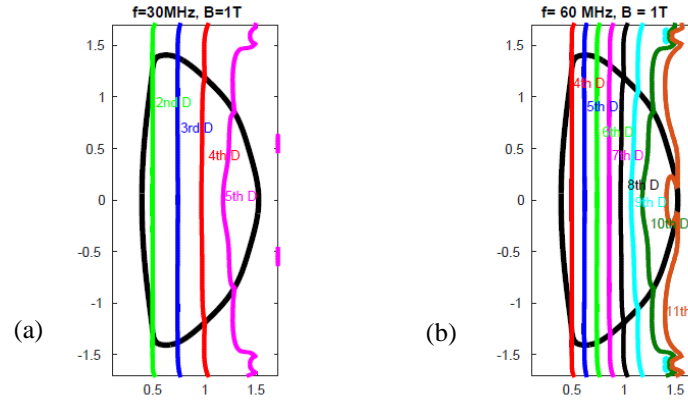


FIG. 3. Deuterium (D) cyclotron resonances for an NSTX-U $B = 1$ T plasma assuming $f = 30$ MHz (Figure (a)) and 60 MHz (Figure (b)).

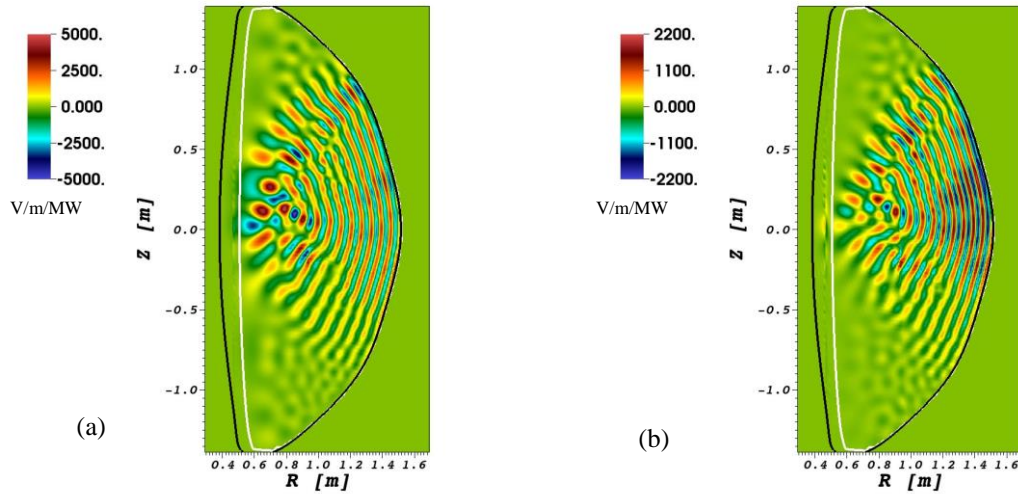


FIG. 4. Real part of the right-handed wave electric field, $Re(E_-)$ (figure (a)) and left-handed wave electric field, $Re(E_+)$ (figure (b)) for an NSTX-U plasma shown in figure 1 for $n_\phi = -12$ and assuming 10% H concentration. The black and white curves represent the last closed flux surface and the fast wave cut-off, respectively.

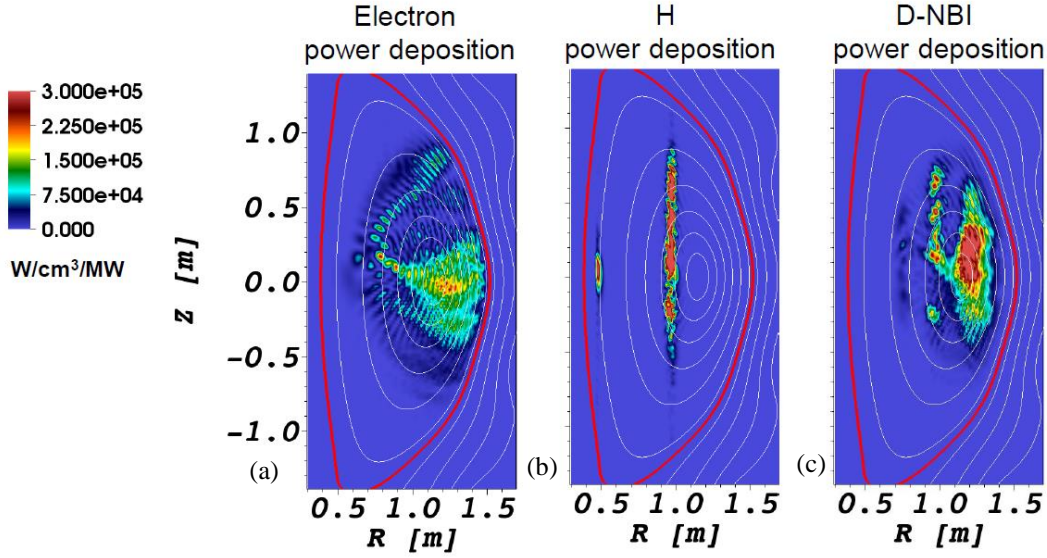


FIG. 5. Contour plots of the electron (a), H (b), and fast ions (c) power deposition for NSTX-U $B_T=1T$ assuming 10% of H concentration for $n_\phi = -12$ and $f=30\text{MHz}$. The red curve represents the last closed flux surface.

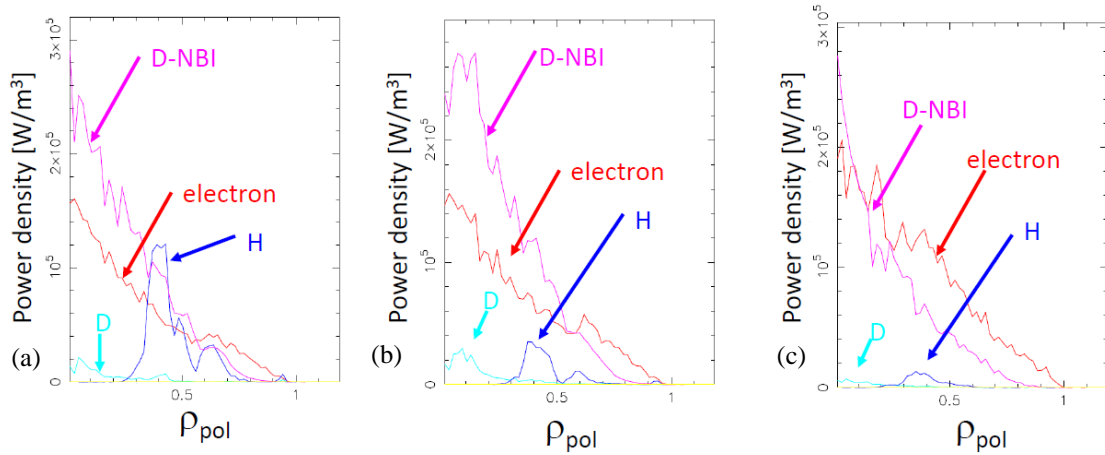


FIG. 6. Flux surface averaged power density power deposition of all plasma species (D, C, H, D-NBI, and electron) as a function of the square root of the normalized poloidal flux, ρ_{pol} . Figure (a): $n_\phi=-12$ and H concentration = 10%; Figures (b) and (c): $n_\phi=-12$ and 21, respectively and H concentration = 2%. Magenta curve represents fast ion absorption, red curve represents electron absorption, blue curve represents H absorption, cyan curve represents thermal D absorption, and yellow curve represents C absorption (which is basically negligible).

It is important to note that the D-NBI absorbed power appears stronger and broader at the fifth harmonic, which is the first resonance the wave electric field encounters during its propagation from the antenna to the core plasma. Figure 6(a) shows the corresponding flux surface averaged power density deposition of all plasma species (D, C, H, D-NBI, and electron) as a function of the square root of the normalized poloidal flux, ρ_{pol} . This figure confirms the peak H absorption localized around the second H harmonic. Moreover, one can see the both electron and fast ions power deposition are peaked on-axis. On the other hand, for this specific case, thermal D is playing a very marginal role and thermal C absorption is essentially zero. As a comparison, figures 6(b) and 6(c) show the flux surface averaged power density deposition as in figure 6(a) assuming 2% H concentration (instead of 10% as shown in figure 6(a) for $n_\phi = -12$ (figure 6(b)) and $n_\phi=-21$ (figure 6(c)). Comparing figures 6(a) and 6(b), a significant reduction of the H absorption is observed due to the reduction of H concentration. However, all other profiles are quite similar between the two figures. Finally, figure 6(c) shows an additional reduction of the H absorption due to the higher wave toroidal number, which typically increases the electron Landau damping due to a slower wave phase velocity.

2.4. Hydrogen concentration scan

In this section we perform a hydrogen concentration scan (1, 2, 5, and 10%) for the NSTX-U plasma shown in figure 1. This scan is carried out for three toroidal wave numbers ($n_\phi = -5, -12, -21$), which represent the dominant n_ϕ components of the HHFW antenna for three different antenna phases. We also consider NSTX-U plasma scenarios with or without NBI. Figures 7 and 8 show the absorption (in percentage) of electrons, thermal deuterium (D), and beam ions (D_{beam}) as a function of the H concentration. Figure 7 (8) is for $f=30$ MHz ($f=60$ MHz). In the first row (second row) of both figures the fast ions are (are not) present. Moreover, first, second, and third columns show the results for $n_\phi = -5, -12, \text{ and } -21$, respectively. From these results we can make some observations: (i) the H absorption is increasing with the H concentration, as expected; (ii) the H absorption can play a significant role for lower n_ϕ in the presence of NBI; (iii) without NBI, H absorption can be up to 60% for $n_\phi = -5$ and 10% H concentration; (iv) for $f=60$ MHz, the H role is quite marginal due to the stronger electron damping and the presence of higher H cyclotron resonances in the plasmas (both with and without NBI). Overall, the electron absorption increases with n_ϕ and it tends to be dominant particularly without NBI. This aspect is even more evident for $f=60$ MHz. The role of fast ions can be quite significant for lower n_ϕ ($|n_\phi| \leq 12$) for both wave frequencies. It is interesting to note that the fast ions absorption is larger for $f=60$ MHz than $f=30$ MHz although in the latter case we have lower D cyclotron resonances. This is attributed to the fact that, for $f=60$ MHz, the wave electric field sees a larger number of D cyclotron resonances with respect to the $f=30$ MHz case (see figures 2 and 3). Even the thermal D absorption can be quite significant for low n_ϕ without NBI. For 2% H concentration, which is a reasonable amount representing the H population in previous NSTX experiments, the impact of the H species can be then important particularly for $f=30$ MHz, lower n_ϕ , and without NBI. From the operational point of view, these results suggest the possibility of using HHFW system in NSTX-U for different purposes and scenarios. In fact, the H power absorption localized to the second harmonic might modify the ion temperature locally and the location can change accordingly to the magnetic field value (see next section). On the other side, due to the high-energy (non-Maxwellian) tail of the H distribution function (caused by the acceleration of H species by HHFW), part of the H absorbed power could be transferred to electron heating via collisions, providing additional core electron heating (beyond the direct electron Landau damping) to the “standard” HHFW performance. This aspect is not analysed here but it will be a subject of a future work. However, these numerical simulations suggest also the possibility to perform HHFW experiments in NSTX-U with H gas puff.

2.5. Hydrogen absorption for different toroidal magnetic field values

A toroidal magnetic field scan is performed in order to cover different scenarios: from NSTX cases ($B_T(0) \approx 0.5$ T) to cases in which we have the second, third, and fourth H cyclotron resonances or only the second harmonic in the plasma. From the experimental point of view, a magnetic field scan results in changes in location of the H cyclotron resonances, which in turn can provide different H localized absorbed power in the plasma which could modify either the electron and/or ion temperature. This is of particular interest also for transport studies. Figure 9 shows the absorption (in percentage) of electrons, thermal deuterium (D), thermal carbon (C), and fast ions (D_{beam}) as a function of the wave toroidal number, n_ϕ for $f=30$ MHz without NBI and four different magnetic equilibria with different magnetic field amplitude. More specifically, we used four different magnetic equilibrium files (“eqdsk”) with a central toroidal magnetic field value corresponding to $B_T(0)=0.53$ T (figure (a)), $B_T(0)=0.63$ T (figure (b)), $B_T(0)=0.76$ T (figure (c)), and $B_T(0)=1$ T (figure (d)). The former case, it corresponds to a NSTX case whereas the latter case corresponds to the cases analyzed in the previous sections. In addition, the $B_T=0.63$ T case is a NSTX-U experiment performed during the initial NSTX-U research operations in 2016 [2-4]. For all these cases a 2% H concentration is considered and the kinetic profiles are the same profiles used in Section 2 (see figures 1(b) and 1(c)). From figure 9 one can note that (i) H absorption decreases with increasing n_ϕ ; (ii) H absorption tends to increase with higher B_T , except for $B_T=0.63$ T; (iii) for $n_\phi=-21$, the electron damping is dominant and the H species does not play any role; (iii) for $n_\phi=-5$ and $B_T=1$ T, the thermal D absorption is up to 20%.

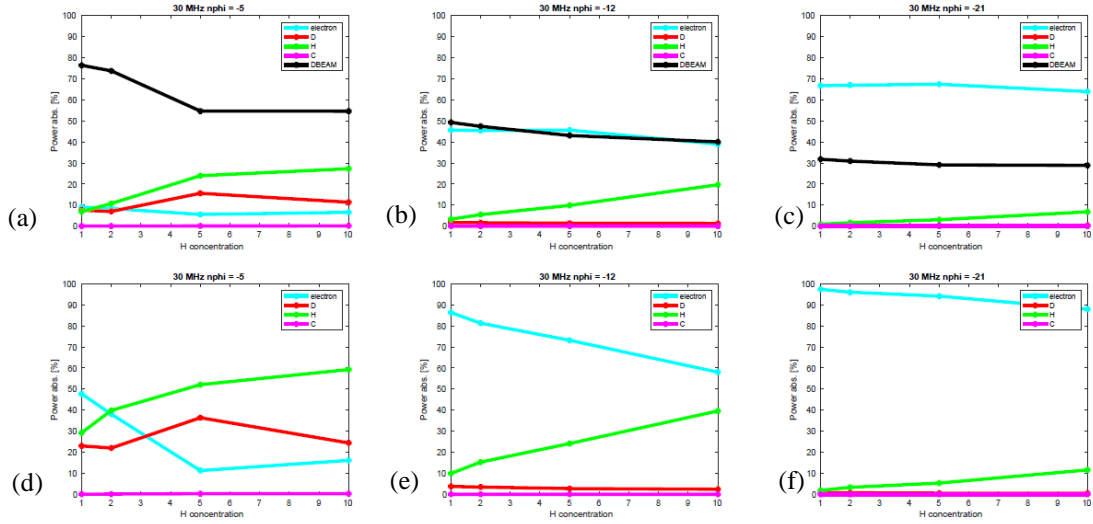


FIG. 7. Absorption of electrons, thermal deuterium (D), thermal hydrogen (H), thermal carbon (C), and fast ions (D_{beam}) as a function of the H concentration (1, 2, 5, and 10%) for NSTX-U plasma assuming $f = 30$ MHz. First row includes a fast ions population whereas second row fast ions are not present. Moreover, first, second, and third column shows the results for $n_\phi = -5, -12,$ and -21 , respectively. Black curves represent fast ion absorption, green curves represent H absorption, red curves represent thermal D absorption, and magenta curves represent C absorption (which is basically negligible).

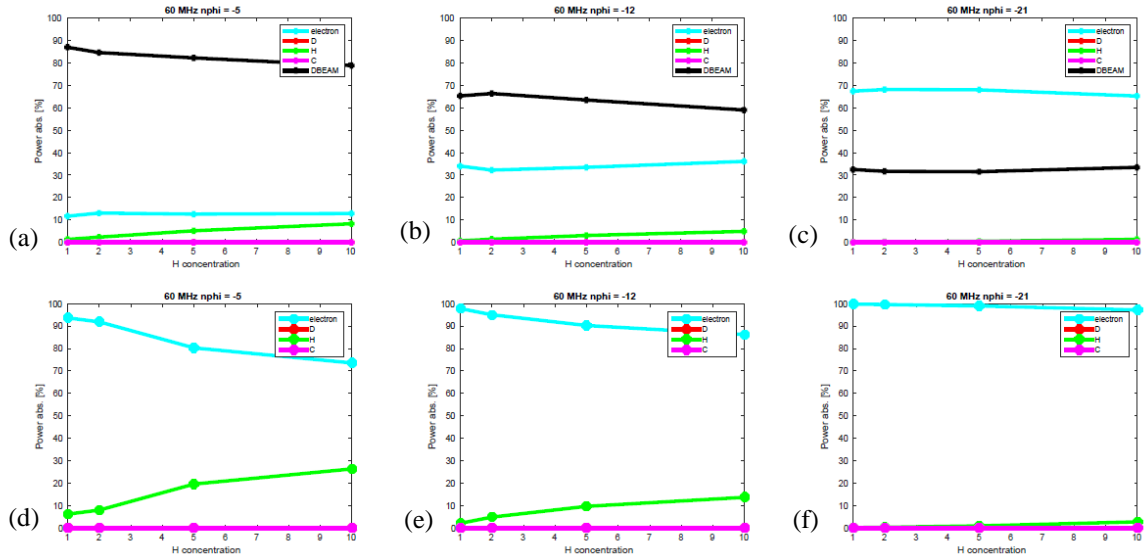


FIG. 8. Absorption of electrons, thermal deuterium (D), thermal hydrogen (H), thermal carbon (C), and fast ions (D_{beam}) as a function of the H concentration (1, 2, 5, and 10%) for NSTX-U plasma assuming $f = 60$ MHz. First row includes a fast ions population whereas second row fast ions are not present. Moreover, first, second, and third column shows the results for $n_\phi = -5, -12,$ and -21 , respectively. Black curves represent fast ion absorption, green curves represent H absorption, red curves represent thermal D absorption, and magenta curves represent C absorption (which is basically negligible).

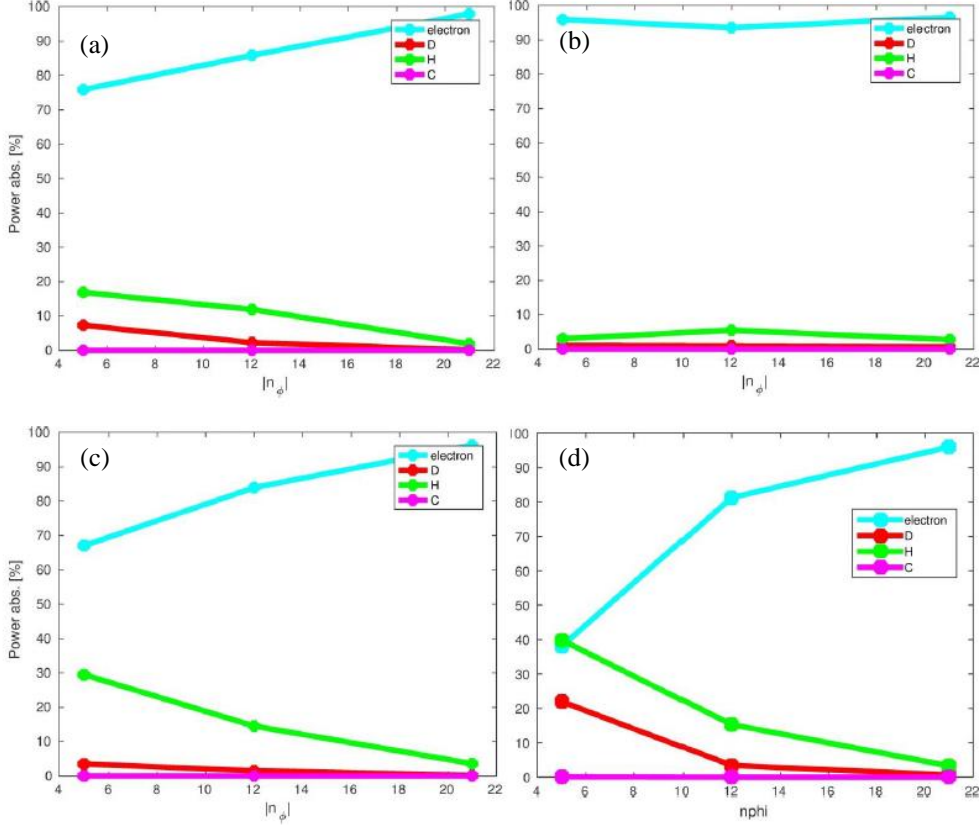


FIG. 9. Absorption of electrons, thermal deuterium (D), thermal carbon (C), and fast ions (D_{beam}) as a function of the wave toroidal number, n_ϕ for $f=30$ MHz without NBI and four different magnetic equilibria: $B_T(0)=0.53$ T (figure (a)), $B_T(0)=0.63$ T (figure (b)), $B_T(0)=0.76$ T (figure (c)), and $B_T(0)=1$ T (figure (d)).

3. CONCLUSIONS AND FUTURE WORK

In this work we performed a series of full wave simulations by making use of the AORSA code for NSTX-U scenarios with $B_T=1$ T in order to investigate the impact of the H species on HHFW performance in NSTX-U plasmas. Different toroidal wave number ($n_\phi = -5, -12, -21$), which represent the dominant n_ϕ components of the HHFW antenna for three different antenna phases, were considered. Moreover, two wave frequencies were adopted: $f=30$ MHz, which corresponds to the current wave frequency in HHFW system used in NSTX and $f=60$ MHz, which would reproduce similar harmonic resonance conditions existed in NSTX in terms of H & D cyclotron resonances in the plasma. We also consider scenarios with and without NBI and we performed a scan in the H concentration. Finally, different magnetic field equilibria and values have been adopted in the simulations.

For $B_T=1$ T scenario, we found an H absorption localized around the second H harmonic, unlike the broad electron and fast ion power depositions. From the H concentration scan we found that (i) the H absorption is increasing with the H concentration, as expected; (ii) the H absorption can play a significant role for lower n_ϕ in the presence of NBI; (iii) without NBI, H absorption can be up to 60% for $n_\phi = -5$ and 10% H concentration; (iv) for $f=60$ MHz, the H role is quite marginal due to the stronger electron damping and the presence of higher H cyclotron resonances in the plasmas (both with and without NBI). In general, the electron absorption increases with n_ϕ and it tends to be dominant particularly without NBI. However, a strong interaction with the fast ions is found for lower n_ϕ ($|n_\phi| \leq 12$) with both wave frequencies (larger for 60 MHz). For 2% H concentration of 2%, which is a reasonable amount representing the H population in previous NSTX experiments, the impact of the H species can be important particularly for $f=30$ MHz, lower n_ϕ , and without NBI. With NBI, electron and fast ions absorptions compete with each other with respect to the antenna phase adopted. For $|n_\phi|=21$, the electron damping is dominant whereas for lower n_ϕ fast ion damping is stronger. The electron damping is even stronger

for $f=60$ MHz without NBI (even for lower n_ϕ). Finally, the H absorption tends to increase with higher toroidal magnetic field due to the presence of the second cyclotron resonance in the core plasma.

In view of future HHFW experiments in NSTX-U, these numerical results suggest the possibility of using HHFW to modify the ion temperature locally. Moreover, part of the H absorbed power could be transferred to electron heating via collisions, providing additional core electron heating (beyond the direct electron Landau damping) to the “standard” HHFW performance due to the high-energy (non-Maxwellian) tail of the H distribution function. This aspect will be investigated in detail in a future work with the use of the full wave AORSA code coupled to the Fokker-Planck code CQL3D. Furthermore, these numerical results will be of course validated with the future NSTX-U experimental campaign.

ACKNOWLEDGEMENTS

This work is supported by U.S. DOE Contract No. DE-AC02-09CH11466. This research used also resources of the National Energy Research Scientific Computing Center (NERSC), a U.S. Department of Energy Office of Science User Facility operated under Contract No. DE-AC02-05CH11231.

REFERENCES

- [1] MENARD, J. E., et al., Nucl. Fusion **52**, 083015 (2012).
- [2] MENARD, J. E., et al., Nucl. Fusion **57**, 102006 (2017).
- [3] BATTAGLIA, D.J., et al., Nucl. Fusion **58**, 046010 (2018).
- [4] KAYE, S. M., et al., “NSTX-U theory, modelling and analysis results”, IAEA Fusion Energy Conference 2018.
- [5] ONO, M., Phys. Plasmas **2**, 4075 (1995).
- [6] HOSEA, J. C., et al., Phys. Plasmas **15**, 056104 (2008).
- [7] MAZZUCATO, E., et al., Phys. Rev. Lett. **101**, 075001 (2008).
- [8] YUH, H., et al., Phys. Rev. Lett. **106**, 055003 (2011).
- [9] TAYLOR, G., et al., 2010 Phys. Plasmas **17**, 056114 (2010).
- [10] JAEGER, E.F., et al., Phys. Plasmas **8**, 1573 (2001).
- [11] GREEN, D. L., et al., Phys. Rev. Lett. **107**, 145001 (2011).
- [12] BERTELLI, N., et al., Nucl. Fusion **56**, 016019 (2016).
- [13] BERTELLI, N., et al., Nucl. Fusion **54**, 083004 (2014).
- [14] LAU, C., et al., Nucl. Fusion **58**, 066004 (2018).
- [15] BERRY, L. A., et al., Phys. Plasmas **23**, 102504 (2016).
- [16] HAWRYLUK, R. J. Physics Close to Thermonuclear Conditions, vol 1 ed B. Coppi *et al* (Brussels: Commission of the European Communities) p 19 (1980).
- [17] GERHARDT, S. P., Nucl. Fusion **52**, 083020 (2012).
- [18] WILSON, J. R., et al., Phys. Plasmas **10**, 1733 (2003).
- [19] LIU, D., et al., Plasma Phys. Control. Fusion **52**, 025006 (2010).